DIGITAL GABOR FILTERS WITH MRA STRUCTURE*

HUI JI†, ZUOWEI SHEN†, AND YUFEI ZHAO†

Abstract. Digital Gabor filters are indispensable tools of local time-frequency analysis in signal processing. With strong orientation selectivity, discrete (tight) Gabor frames generated by 2D Gabor filters also see their wide applications in image processing and volume data processing. However, owing to the lack of multi-scale structures, discrete Gabor frames are less effective than multi-resolution analysis (MRA) based wavelet (tight) frames when being used for modeling data composed of local structures with varying sizes. Recently, it is shown that digital Gabor filters do generate MRA-based wavelet tight frames via Unitary Extension Principle. However, the corresponding window function has to be constant window, which has poor joint time-frequency resolution. In this paper, we showed that digital Gabor filters with smooth window function can generate MRA-based wavelet bi-frames. The MRA-based wavelet bi-frames generated by digital Gabor filters have both the advantages of Gabor systems on local time-frequency analysis and the advantages of wavelet systems on multi-scale analysis.

Key words. Multi-scale analysis, Local time-frequency analysis, Bi-frames, Wavelets

AMS subject classifications. 42A16, 42C40, 65T60

1. Introduction. For years, digital Gabor filters and their associated digital Gabor systems [18] have long been known as the pervasive tools of local time-frequency analysis in audio processing, texture analysis, image analysis and many others (see e.g. [2, 13, 20]). A Gabor system is generated by the translations and modulations of a window function g:

$$X = \{g(\cdot - ak)e^{i2\pi b\ell\cdot}\}_{k,\ell\in\mathbb{Z}}, \tag{1}$$

where a, b are shift parameters. The main reason of choosing Gabor systems over others is its optimality on joint time-frequency resolution, when Gaussian functions are used as the window function of Gabor systems. Recently, motivated by strong orientation selectivity of tensor product of digital Gabor filters, discrete Gabor (tight) frames also have been proposed in [23] for efficient sparse approximation of high-dimensional data. A class of (tight) discrete Gabor frames for finite signals are constructed in [23] whose corresponding filter bank maximizes orientation selectivity in discrete grid. Such discrete Gabor frames show their advantages over many widely used systems, e.g. spline wavelet tight frames [11], when being used in various applications.

It can be seen from (1) that Gabor (tight) frames lack the so-called multi-scale structures, one very important property needed for effectively modeling local structures in signals with varying sizes. Indeed, such a weakness of Gabor systems was the motivation of studying affine (wavelet) systems. For $L_2(\mathbb{R})$, a dyadic wavelet system can be expressed as

$$\{2^{n/2}\psi_\ell(2^n\cdot - k)\}_{1\le\ell\le r,n,k\in\mathbb{Z}}. \tag{2}$$

Multi-scale structures of wavelet systems allow one to decompose signals into multiple levels with different scales, which is very helpful to model local structures existing in signals with varying sizes. Together with fast cascade filter bank based implementation of signal decomposition/reconstruction, multi-resolution analysis (MRA) based wavelet tight frames [11, 32] have been used in a wide range of applications (see e.g. [3, 4, 15, 16, 26, 36]). Therefore, it is natural to ask whether it is possible to have discrete tight frames

*Submitted to the editors.

Funding: This work was funded by the Singapore MOE Academic Research Fund Tier 3 (MOE2012-T3-1-008) and the Singapore MOE Academic Research Fund Tier 1 (R-146-000-229-114)

†Department of Mathematics, National University of Singapore, (matjh@nus.edu.sg,matzuows@nus.edu.sg,matzyf@nus.edu.sg.

that have both affine structures associated with an MRA and local time-frequency analysis. Such a question can be rephrased as whether we can have MRA-based wavelet tight frames whose corresponding wavelet filter bank is a set of digital Gabor filters.

Based on Unitary Extension Principle (UEP) [11, 32], the question above is addressed in [24], which showed that digital Gabor filters indeed can generate an MRA-based wavelet tight frame for $L_2(\mathbb{R})$. However, it only works for those Gabor filters with constant window function, i.e. $g = M^{-1}[1, 1, \ldots, 1]$, where M is the length of g. It is known that a constant window function is not smooth in time domain, and thus has very slow decay in frequency domain. As a result, the joint time-frequency resolution of such wavelet tight frames is much more limited than that of Gabor systems with smooth window functions.

The results above naturally raise the following question: can we have wavelet systems with all nice properties of wavelet tight frames that are closely connected to digital Gabor filters with smooth window function? Our answer to this question is the study of MRA-based wavelet bi-frames. In this paper, we showed that it is possible to have MRA-based wavelet bi-frames generated by digital Gabor filters with fast decay in frequency domain. Such wavelet bi-frames have both good joint time-frequency resolution and MRA-based multi-scale structure. The MRA-based wavelet bi-frames also have the same fast discrete implementation of signal decomposition/reconstruction as wavelet tight frames. Based on Mixed Extension Principle [17], the wavelet frames and their dual frames of the constructed MRA-based wavelet bi-frames are both generated by some Gabor-induced digital filter bank with fast decay in frequency domain. With the best from both Gabor systems and wavelet systems, the wavelet bi-frames constructed in this paper certainly can see their applications in many signal/image processing tasks.

1.1. Related work. We first introduce some definitions related to Gabor systems and wavelet systems. For the space $L_2(\mathbb{R})$, a Gabor system $X \subset L_2(\mathbb{R})$ is generated by the translations and modulations of a window function $g \in L_2(\mathbb{R})$:

$$X = (K, L)_g = \{g(x-u)e^{i2\pi\eta x}\}_{u\in K,\eta\in L},$$

where $K \times L \in \mathbb{R} \times \mathbb{R}$ is a lattice. A p-dilation wavelet system $X(\Psi) \subset L_2(\mathbb{R})$ is composed of the dilations and translations of a set of wavelets $\Psi = \{\psi_1, ..., \psi_r\}$:

$$X(\Psi) = \{p^{n/2}\psi_\ell(p^n \cdot -k)\}_{1\le\ell\le r,n,k\in\mathbb{Z}}.$$

For the space $\ell_2(\mathbb{Z})$, a discrete Gabor system $X \subset \ell_2(\mathbb{Z})$ is obtained via uniformly sampling a Gabor system in $L_2(\mathbb{R})$:

$$\{g(m-ak)e^{2\pi ib\ell m}, m \in \mathbb{Z}\}_{k\in\mathbb{Z},\ell\in\{0,\ldots,\frac{1}{b}-1\}}, \tag{3}$$

where a, b with $a, \frac{1}{b} \in \mathbb{Z}^+$ are shift parameters. The b^{-1} atoms $\{g(m)e^{2\pi ib\ell m}\}_{0\le\ell\le\frac{1}{b}-1}$ are often called *digital Gabor filters*. The construction of discrete wavelet systems is different from the construction of discrete Gabor systems. Consider an MRA-based wavelet tight frame $X(\Psi)$. Let ϕ denote the p-refinable function that generates an MRA:

$$\phi(x) = p\sum_{k\in\mathbb{Z}} a_0(k)\phi(px-k), \quad x \in \mathbb{R},$$

where the sequence a_0 is called the *refinement mask* of ϕ. The wavelets $\Psi = \{\psi_\ell\}_{\ell=1}^r$ are then defined by

$$\psi_\ell(x) = p\sum_{k\in\mathbb{Z}} a_\ell(k)\phi(px-k), \quad x \in \mathbb{R},\ 1 \le \ell \le r,$$

where the sequences $\{a_\ell\}_{\ell=1}^r$ are called the *wavelet masks* of Ψ. Discrete wavelet tight frame for $\ell_2(\mathbb{Z})$ is then constructed using the set of refinement and wavelet masks $\{a_\ell\}_{\ell=0}^r$, the so-called wavelet filter bank; see e.g. [36].

There has been an abundant literature on frames. A complete survey of the literature goes beyond the scope of this paper. Instead, we only mention the duality analysis for frames. Duality analysis for shift-invariant space is developed in $L_2(\mathbb{R}^d)$ [34] via dual Gramian analysis. This leads to the discovery of the duality principle for Gabor systems [30, 33] and the UEP [31] for MRA-based wavelet tight frames and bi-frames. Both the duality principle and the unitary extension principle lead to simple construction scheme of Gabor frames and wavelet frames. The Duality analysis for general Hilbert space can be found in [17]. It unifies the duality principle for Gabor systems and the Unitary Extension Principle for wavelet systems, and leads to the discovery that digital Gabor filters do form MRA-based wavelet frames.

There are also other construction schemes for Gabor frames. Interested readers are referred to [6, 9, 27, 33] for more details on the construction of Gabor frames for $L_2(\mathbb{R})$ and [22, 23, 38, 40] for more details on the construction of Gabor (tight) frames for $\ell_2(\mathbb{Z})$ or $\mathbb{C}^N$. The key of the construction is the duality principle ([12, 17, 21, 30, 33]), which not only gives a characterization of frame properties, but also provides basic principle for the construction. For the construction of Gabor window functions, the famous painless construction [10] is the most important one, which appeared earlier than duality principle but can be viewed as one application of duality principle. Many other constructions of Gabor window functions are related to the main idea of duality principle.

For wavelet systems, the construction took off after the discovery of multi-resolution analysis by Mallat and Meyer [28, 29]. Since then, many types of wavelet bases have been constructed, i.e., band-limited orthonormal wavelet bases by Meyer [29], compactly supported orthonormal wavelet bases by Daubechies [8], and biorthogonal wavelet bases [7]. Duality analysis for shift-invariant subspace developed in $L_2(\mathbb{R}^d)$ [34] leads to the discovery of UEP [31] for MRA-based wavelet tight frames and bi-frames. Duality analysis for general Hilbert space can be found in [17]. Compactly supported spline wavelet tight frames constructed in [31] are the first set of examples of MRA-based tight frames generated by the UEP. Under very mild conditions, the UEP simplifies the verification of tight frame property of a wavelet system to the verification of only a few constraints on the associated filter bank. The extension of the UEP to the case of MRA-based wavelet bi-frames is presented in [30, 33], the so-called *Mixed Extension Principle* (MEP). Based on MEP, a simple construction scheme of MRA-based wavelet bi-frame is developed in [17], which only involves the explicit construction of an invertible matrix and its inverse.

The studies of introducing multi-scale structure to Gabor systems are scant in the existing literature. In [25], Gabor wavelet transform for $L_2(\mathbb{R})$ is defined by using Gabor functions as the mother wavelet function of the continuous wavelet transform. Then, a discrete system for $L_2(\mathbb{R})$ with both Gabor structure and multi-scale structure can be obtained by directly sampling the phase. It is empirically observed that the resulting system will form a frame for $L_2(\mathbb{R})$, as long as the sampling in the phase domain is dense enough. However, such systems cannot introduce discrete Gabor (tight) frames for the sequence space $\ell_2(\mathbb{Z})$, and have no fast cascade algorithm as MRA-based wavelet tight frame either. A class of discrete Gabor (tight) frames for $\ell_2(\mathbb{Z})$ is constructed in [23], and multi-scale structure is introduced by considering a (tight) frame composed of multiple discrete Gabor (tight) frames with different window sizes. Similarly, such discrete Gabor (tight) frames for $\ell_2(\mathbb{Z})$ have no fast cascade algorithm.

The gap between MRA-based wavelet tight frames and Gabor systems motivated the study on MRA-based wavelet tight frames generated by the set of digital Gabor filters [24]. It is shown in [24] that the set of digital Gabor filters satisfies the UEP, only if the window function is a constant function. In other words, in order to form an MRA-based wavelet tight frame for $L_2(\mathbb{R})$, the only choices of digital Gabor filters are those with constant windows. As a constant window is not smooth and thus has a slow decay in frequency

domain, these Gabor filters have poor joint time-frequency resolution. As a result, such systems lose the main motivation of Gabor systems, i.e., the optimality on joint time-frequency resolution.

1.2. Main results. In this paper, we showed that it is possible to have MRA-based wavelet bi-frames generated by digital Gabor filters with fast decay in frequency domain, which will have both multi-scale structure and fast cascade implementation of signal reconstruction/decomposition, while keeping the good joint time-frequency resolution. Recall that the construction of MRA-based wavelet frames usually starts with the construction of a p-refinable function ϕ that generates an MRA for $L_2(\mathbb{R})$. For simplicity, only compactly supported refinable functions are considered in this paper.

Suppose that we have two refinable functions $\phi, \widetilde{\phi}$ with refinable masks $a_0, \widetilde{a}_0$, and each of them generates an MRA for $L_2(\mathbb{R})$. Define two sets of framelets $\Psi = \{\psi_\ell\}_{\ell=1}^r, \widetilde{\Psi} = \{\widetilde{\psi}_\ell\}_{\ell=1}^r$ as follows,

$$\psi_\ell(\cdot) = p\sum_{k\in\mathbb{Z}} a_\ell(k)\phi(p\cdot -k); \quad \widetilde{\psi}_\ell(\cdot) = p\sum_{k\in\mathbb{Z}} \widetilde{a}_\ell(k)\widetilde{\phi}(p\cdot -k),$$

for $\ell = 1, \ldots, r$. Then, these two sets of framelets can be used to generate two wavelet systems:

$$X(\Psi) = \{p^{n/2}\psi_\ell(p^n\cdot -k)\}_{1\le\ell\le r;n,k\in\mathbb{Z}}; \quad X(\widetilde{\Psi}) = \{p^{n/2}\widetilde{\psi}_\ell(p^n\cdot -k)\}_{1\le\ell\le r;n,k\in\mathbb{Z}}.$$

The MEP [17] provides an approach for constructing MRA-based wavelet bi-frames via their refinement masks and wavelet masks. The MEP says that under very mild conditions, the two systems $X(\Psi), X(\widetilde{\Psi})$ form bi-frames for $L_2(\mathbb{R})$, if the two mask sets $\{a_\ell\}_{\ell=0}^r$ and $\{\widetilde{a}_\ell\}_{\ell=0}^r$ satisfy

$$\sum_{\ell=0}^{r} \widehat{a_\ell}(\omega)\overline{\widehat{\widetilde{a}_\ell}(\omega+2\pi\nu)} = \delta_{\nu,0}, \tag{4}$$

for all $\nu \in p^{-1}\mathbb{Z}/\mathbb{Z}$ and a.e. $\omega \in \mathbb{R}$.

Using the MEP as the main tool, we can then construct MRA-based wavelet bi-frames generated by digital Gabor filters. Consider a discrete Gabor system of the form (3) with $M(=b^{-1})$ Gabor filters:

$$g_\ell(m) = g(m)e^{-2\pi i\ell bm}, \quad \ell = 0, 1, \ldots, M-1,$$

where g is a compactly supported non-negative sequence in $\ell_2(\mathbb{Z})$ with $\mathrm{supp}(g) \subset [0, M-1]\cap\mathbb{Z}$. Define the following two set of masks $\{a_\ell\}_{\ell=0}^{M-1}$ and $\{\widetilde{a}_\ell\}_{\ell=0}^{M-1}$:

$$\begin{cases} a_0(m) = g_0(m), \\ a_\ell(m) = e^{i\theta_\ell}g_\ell(m) - \mu_\ell g_0(m),\ 1\le\ell\le M-1; \end{cases} \quad \begin{cases} \widetilde{a}_0(m) = g_0(m), \\ \widetilde{a}_\ell(m) = be^{i\theta_\ell}e^{-2\pi ib\ell m},\ 1\le\ell\le M-1, \end{cases} \tag{5}$$

where $e^{i\theta_\ell} = \frac{\overline{\sum_m g_\ell(m)}}{|\sum_m g_\ell(m)|}$, $\mu_\ell = \frac{|\sum_m g_\ell(m)|}{\sum_m g_0(m)}$ if $\sum_m g_\ell(m) \neq 0$; and $\theta_\ell = \mu_\ell = 0$ otherwise. It can be seen that in (5), the two refinement masks $a_0, \widetilde{a}_0$ are the same. The wavelet mask set $\{a_\ell\}_{\ell=1}^{M-1}$ is constructed by removing possible non-zero DC offset of digital Gabor filters (a common implementation in practice). Then, we showed that the two mask sets $\{a_\ell\}_{\ell=0}^{M-1}$ and $\{\widetilde{a}_\ell\}_{\ell=0}^{M-1}$ defined by (5) satisfy the MEP (4) and thus generate wavelet bi-frames for $L_2(\mathbb{R})$, if the window sequence g satisfies

$$\sum_{n\in\mathbb{Z}} g(j+pn) = \frac{1}{p}, \quad \forall\, j \in \mathbb{Z}/p\mathbb{Z}, \tag{6}$$

where $p \in \mathbb{Z}$ and $p > 1$.

Based on the construction scheme above, several examples of MRA-based wavelet bi-frames are constructed using different window sequences g that satisfy (6), include both the discretization of B-spline functions and the refinement mask of B-spline functions. The extension to the high-dimensional case is also straightforward, and we give an example that is based on the discretization of box-spline functions. In addition, the frame bound ratios of the resulting discrete wavelet bi-frames for signal space are also examined in this paper, and the results show that the frame bound ratios of these bi-frames are quite small and thus there is no concern on numerical stability of signal decomposition and reconstruction. At last, the constructed MRA-based wavelet bi-frames are used in several sparsity-based image recovery tasks. It is empirically observed that the constructed wavelet bi-frames outperform some widely used systems such as B-spline wavelet tight frames and dual-tree complex wavelet transform (DT-CWT).

The remainder of this paper is organized as follows. Some related background and mathematical preliminaries are introduced in Section 2. Section 3 is mainly devoted to the construction of MRA-based wavelet bi-frames generated by digital Gabor filters, as well as several examples. Section 4 is about discussing discrete wavelet bi-frames for signals derived from MRA-based wavelet tight frames for $L_2(\mathbb{R})$, and their frame bound ratios, which are related to the stability in signal decomposition and reconstruction. At last, in Section 5, the constructed wavelet bi-frames are tested in various image recovery tasks with the comparison to some widely used frames in image processing.

2. Preliminaries. In this paper, let $\mathbb{Z}, \mathbb{Z}^+, \mathbb{R}, \mathbb{C}$ denote the set of integers, positive integers, real numbers and complex numbers, respectively. Let $\langle \cdot, \cdot \rangle$ and $\|\cdot\|$ be the usual inner product and norm of the Hilbert space H. The Fourier transform of $f \in L_2(\mathbb{R})$ is denoted by $\widehat{f}$; and for $f \in L_1(\mathbb{R}) \cap L_2(\mathbb{R})$, $\widehat{f}$ is defined by

$$\widehat{f}(\xi) = \int_{\mathbb{R}} f(x) e^{-i\xi x} dx, \quad \xi \in \mathbb{R}.$$

The Fourier transform of $h \in \ell_2(\mathbb{Z})$ is also denoted by $\widehat{h}$ and is defined by

$$\widehat{h}(\xi) = \sum_{k \in \mathbb{Z}} h(k) e^{-ik\xi}, \quad \xi \in \mathbb{R}.$$

Let I denote any countable index set, a sequence $\{v_n\}_{n \in I} \subset H$ is called a *Bessel* sequence if there exists a positive constant B such that

$$\sum_{n \in I} |\langle f, v_n \rangle|^2 \leq B \|f\|^2, \quad \forall\, f \in H.$$

A sequence $\{v_n\}_{n \in I} \subset H$ is called a *frame* if there exist two positive constant A, B such that

$$A\|f\|^2 \leq \sum_{n \in I} |\langle f, v_n \rangle|^2 \leq B \|f\|^2, \quad \forall\, f \in H.$$

A/B is called the lower/upper frame bound. A frame $\{v_n\}_{n \in I}$ is called *tight frame* when $A = B = 1$. Given a frame $\{u_n\}_{n \in I}$ for H, the sequence $\{v_n\}_{n \in I}$ is called its *dual frame* if

$$f = \sum_{n \in I} \langle f, v_n \rangle u_n = \sum_{n \in I} \langle f, u_n \rangle v_n, \quad \forall\, f \in H. \tag{7}$$

For a tight frame, one of its dual frames is the tight frame itself. A frame $\{u_n\}_{n \in I}$ and its dual $\{v_n\}_{n \in I}$ are called *bi-frames* for H.

Given a Bessel sequence $\{v_n\}_{n\in I} \subset H$, its *analysis operator* $W_v : H \to \ell_2(I)$ is defined by

$$W_v f(n) = \langle f, v_n\rangle, \quad n \in I,$$

for any $f \in H$. Its adjoint operator $W_v^* : \ell_2(I) \to H$ is then defined by

$$W_v^* c = \sum_{n\in I} c_n v_n, \quad \forall\, \{c_n\}_{n\in I} \in \ell_2(I).$$

The operator W_v^* is also called *synthesis operator*. The Bessel sequences $\{u_n\}_{n\in I}$ and $\{v_n\}_{n\in I}$ form bi-frames for H if and only if $W_v^* W_u = W_u^* W_v = I$.

Consider a p-refinable function $\phi \in L_2(\mathbb{R})$ with $\widehat{\phi}(0) \neq 0$ that satisfies

$$\phi(x) = p\sum_{k\in\mathbb{Z}} a_0(k)\phi(px-k), \quad x \in \mathbb{R}, \tag{8}$$

or equivalently $\widehat{\phi}(p\xi) = \widehat{a_0}(\xi)\widehat{\phi}(\xi), \xi \in \mathbb{R}$, for some refinement mask $a_0 \in \ell_2(\mathbb{Z})$. We define a sequence of subspaces generated by ϕ:

$$V_n = \overline{span\{\phi(p^n\cdot -k)\}}_{k\in\mathbb{Z}}. \tag{9}$$

The sequence of subspaces $\{V_n\}_{n\in\mathbb{Z}} \subset L_2(\mathbb{R})$ forms an MRA if

$$\text{(i) } V_n \subset V_{n+1},\ n \in \mathbb{Z}, \quad \text{(ii) } \overline{\cup_n V_n} = L_2(\mathbb{R}), \quad \text{(iii) } \cap_n V_n = \{0\}.$$

Given an MRA generated by the refinable function ϕ, we can define a set of framelets $\Psi = \{\psi_\ell\}_{\ell=1}^r$ via

$$\psi_\ell(x) = p\sum_{k\in\mathbb{Z}} a_\ell(k)\phi(px-k), \quad x \in \mathbb{R}, \tag{10}$$

or equivalently $\widehat{\psi_\ell}(p\xi) = \widehat{a_\ell}(\xi)\widehat{\phi}(\xi), \xi \in \mathbb{R}$, for wavelet masks $\{a_\ell\}_{\ell=1}^r \subset \ell_2(\mathbb{Z})$. Associated with Ψ, the p-dilation wavelet system $X(\Psi)$ is defined by

$$X(\Psi) = \{p^{n/2}\psi_\ell(p^n\cdot -k)\}_{1\le\ell\le r, n,k\in\mathbb{Z}}. \tag{11}$$

For simplicity, the refinable function $\phi \in L_2(\mathbb{R})$ is assumed to be compactly supported with the finitely supported, real valued refinement mask $a_0 \in \ell_2(\mathbb{Z})$, and suppose ϕ satisfies $\widehat{\phi}(0) = 1$. The Mixed Extension Principle (MEP, [32]) provides a sufficient condition on the masks for two wavelet systems to form bi-frames for $L_2(\mathbb{R})$.

THEOREM 1 (MEP [32]). *Let $\phi, \widetilde{\phi}$ be compactly supported refinable functions with refinement masks $a_0, \widetilde{a}_0$ and $\widehat{\phi}(0) = \widehat{\widetilde{\phi}}(0) = 1$. Let $\{a_\ell\}_{\ell=1}^r$ (resp. $\{\widetilde{a}_\ell\}_{\ell=1}^r$) be the wavelet masks of a wavelet system X derived from ϕ (resp. Y derived from $\widetilde{\phi}$) by (10) and (11). Then, X and Y are dual frames, provided they are Bessel systems and*

$$\sum_{\ell=0}^r \widehat{a}_\ell(\omega)\overline{\widehat{\widetilde{a}}_\ell(\omega+2\pi\nu)} = \delta_{\nu,0}, \quad \text{for a.e. } \omega \in \mathbb{R}$$

for all $\nu \in p^{-1}\mathbb{Z}/\mathbb{Z}$, or equivalently

$$\sum_{\ell=0}^r \sum_{n\in\Omega_j} \overline{a_\ell(n)}\widetilde{a}_\ell(n+k) = \frac{1}{p}\delta_{k,0} \tag{12}$$

for all $k \in \mathbb{Z}$, $j \in \mathbb{Z}/p\mathbb{Z}$, where $\Omega_j = (p\mathbb{Z}+j)$.

REMARK 2. *In Theorem 1, in addition to (12), the only condition imposed on the systems is that both X and Y should be Bessel systems. This condition will be satisfied as long as refinable functions $\phi, \widetilde{\phi} \in L_2(\mathbb{R})$ are compactly supported and each of the wavelet frames from $\{a_\ell\}_{\ell=1}^r, \{\widetilde{a}_\ell\}_{\ell=1}^r$ is finitely supported and has the first order vanishing moment (see e.g. [19]).*

It can be seen that when $X = Y$, the condition (4) is exactly the condition in UEP, i.e.

$$\sum_{\ell=0}^{r} \sum_{n\in\Omega_j} \overline{a_\ell(n)} a_\ell(n+k) = \frac{1}{p}\delta_{k,0}. \tag{13}$$

The main difference between UEP and MEP is that the MEP requires both the conditions (12) and that two systems are Bessel sequences, while the UEP only requires the condition (13).

The MEP simplifies the construction of MRA-based wavelet bi-frames for $L_2(\mathbb{R})$ by converting it to the construction of refinement and wavelet masks that satisfy (12). In [17], a construction scheme of such refinement and wavelet masks is provided for dilation factor $p = 2$, which further simplified the problem by converting it to the problem of completing a constant matrix with explicit form of its inverse. Such an idea is also exploited in the construction of discrete Gabor filters that satisfy (12).

3. Construction of wavelet bi-frames. This section aims at constructing MRA-based wavelet bi-frames whose refinement and wavelet masks are derived from digital Gabor filters. Let $g \in \ell_2(\mathbb{Z})$ be a finitely supported window sequence with $\mathrm{supp}(g) \subset [0, M-1] \cap \mathbb{Z}$. It then generates a set of digital Gabor filters $G = \{g_\ell\}_{\ell=0}^{1/b-1}$:

$$g_\ell(m) = g(m)e^{-2\pi i \ell b m}, \tag{14}$$

where $b(= \frac{1}{M})$ is the frequency shift parameter. In practice, a high-pass digital Gabor filter is usually implemented to have zero DC offset, i.e., the mean of the filter is zero. Such an implementation can be done by removing the DC offset of all high-pass filters as follows,

$$\bar{g}_\ell = e^{i\theta_\ell} g_\ell - \mu_\ell g_0, \quad \forall\, 1 \le \ell < 1/b, \tag{15}$$

where $e^{i\theta_\ell} = \frac{\overline{\sum_m g_\ell(m)}}{|\sum_m g_\ell(m)|}, \mu_\ell = \frac{|\sum_m g_\ell(m)|}{\sum_m g_0(m)}$ if $\sum_m g_\ell(m) \neq 0$, and $\theta_\ell = \mu_\ell = 0$ otherwise. Clearly, we have

$$\sum_{m\in\mathbb{Z}} \bar{g}_\ell(m) = 0, \quad 1 \le \ell < 1/b.$$

It is noted that the property of zero DC offset is exactly the property of first-order vanishing moment, a necessary property of wavelet masks.

Consider a refinement mask $a_0 = g_0$ and wavelet masks $a_\ell = \bar{g}_\ell$, i.e.,

$$\begin{cases} a_0(m) &= g(m), \\ a_\ell(m) &= e^{i\theta_\ell} g_\ell(m) e^{-2\pi i \ell b m} - \mu_\ell g(m), \quad 1 \le \ell < 1/b, \end{cases} \tag{16}$$

for $m \in [0, 1/b-1] \cap \mathbb{Z}$ and 0 otherwise. Define another set of refinement mask and wavelet masks as follows,

$$\begin{cases} \widetilde{a}_0(m) = g(m), \\ \widetilde{a}_\ell(m) = b e^{i\theta_\ell} e^{-2\pi i \ell b m}, \qquad 1 \le \ell < 1/b \end{cases} \tag{17}$$

for $m \in [0, 1/b-1] \cap \mathbb{Z}$ and 0 otherwise. It can be seen that the mean of the sequence $\widetilde{a}_\ell$ is also zero. Define $\Omega_j = (p\mathbb{Z} + j) \cap \mathrm{supp}(g)$ for $j = 0, \ldots, p-1$. Then, we have

THEOREM 3. *Consider a finitely supported, real-valued, nonnegative window sequence $g \in \ell_2(\mathbb{Z})$. Let $\{a_\ell\}_{\ell=0}^{1/b-1}$ and $\{\widetilde{a}_\ell\}_{\ell=0}^{1/b-1}$ be two mask sets defined by (16) and (17). Suppose that for some integer $p > 1$, the window sequence g satisfies*

$$\sum_{n\in\Omega_j} g(n) = p^{-1}, \quad \forall\, j \in \mathbb{Z}/p\mathbb{Z}, \tag{18}$$

where $\Omega_j = (p\mathbb{Z} + j) \cap \mathrm{supp}(g)$. Then, two sets $\{a_\ell\}_{\ell=0}^{1/b-1}$ and $\{\widetilde{a}_\ell\}_{\ell=0}^{1/b-1}$ satisfy the MEP condition (12):

$$\sum_{\ell=0}^{1/b-1} \sum_{n\in\Omega_j} \overline{a_\ell(n)}\widetilde{a}_\ell(n+k) = p^{-1}\delta_{k,0}, \quad \forall\, j \in \mathbb{Z}/p\mathbb{Z}.$$

Proof. Consider any integer $n \in [0, 1/b-1]\cap\mathbb{Z}$. For $k < -n$ or $k > 1/b-1-n$, we have $\widetilde{a}_\ell(n+k) = 0$. Consequently,

$$\sum_{\ell=0}^{1/b-1} \overline{a_\ell(n)}\widetilde{a}_\ell(n+k) = 0 \quad \text{for } k < -n \text{ and } k > \frac{1}{b} - 1 - n. \tag{19}$$

For $-n \le k \le \frac{1}{b} - 1 - n$, by (16) and (17), we have

$$\begin{aligned}\sum_{\ell=0}^{1/b-1} \overline{a_\ell(n)}\widetilde{a}_\ell(n+k) &= g(n)g(n+k) + \sum_{\ell=1}^{1/b-1} \left(e^{-i\theta_\ell} g(n)e^{2\pi i\ell bn} - \mu_\ell g(n)\right)\cdot be^{i\theta_\ell}e^{-2\pi i\ell b(n+k)} \\ &= g(n)g(n+k) + \sum_{\ell=1}^{1/b-1} bg(n)e^{-2\pi i\ell bk} - \sum_{\ell=1}^{1/b-1} b\mu_\ell g(n)e^{i\theta_\ell}e^{-2\pi i\ell b(n+k)}.\end{aligned}$$

Notice that $-n \le k \le \frac{1}{b} - 1 - n$ implies $1 - \frac{1}{b} \le k \le \frac{1}{b} - 1$. Thus,

$$\sum_{\ell=1}^{1/b-1} bg(n)e^{-2\pi i\ell bk} = \begin{cases} (1-b)g(n), & k = 0, \\ -bg(n), & -n \le k \le \frac{1}{b} - 1 - n,\ k \ne 0, \end{cases}.$$

and

$$\begin{aligned}\sum_{\ell=1}^{1/b-1} b\mu_\ell g(n)e^{i\theta_\ell}e^{-2\pi i\ell b(n+k)} &= bg(n) \sum_{\ell=1}^{1/b-1} \overline{\sum_m g_\ell(m)}e^{-2\pi i\ell b(n+k)} \\ &= bg(n) \sum_{m=0}^{1/b-1} g(m) \sum_{\ell=1}^{1/b-1} e^{-2\pi i\ell b(n+k-m)} \\ &= g(n)g(n+k) - bg(n).\end{aligned}$$

Therefore, we have

$$\sum_{\ell=0}^{1/b-1} \overline{a_\ell(n)}\widetilde{a}_\ell(n+k) = \begin{cases} g(n), & k = 0; \\ 0, & -n \le k \le \frac{1}{b} - 1 - n,\ k \ne 0. \end{cases} \tag{20}$$

In other words,

$$\sum_{\ell=0}^{1/b-1} \overline{a_\ell(n)}\widetilde{a}_\ell(n+k) = \begin{cases} g(n), & k=0, \\ 0, & k\in\mathbb{Z},\ k\neq 0. \end{cases}.$$

Then, for $k=0$, by (18), we have

$$\sum_{\ell=0}^{1/b-1}\sum_{n\in\Omega_j} \overline{a_\ell(n)}\widetilde{a}_\ell(n) = \sum_{n\in\Omega_j} g(n) = p^{-1}, \quad \forall\, j\in\mathbb{Z}/p\mathbb{Z}.$$

For $k\neq 0$, we have

$$\sum_{\ell=0}^{1/b-1}\sum_{n\in\Omega_j} \overline{a_\ell(n)}\widetilde{a}_\ell(n+k) = \sum_{n\in\Omega_j}\sum_{\ell=0}^{1/b-1} \overline{a_\ell(n)}\widetilde{a}_\ell(n+k) = 0, \quad \forall\, j\in\mathbb{Z}/p\mathbb{Z}.$$

The proof is complete. □

Now, suppose that we have in hand such a window sequence g satisfying the condition (18). Define a p-refinable function (or distribution) ϕ by

$$\phi(\cdot) = p\sum_{m\in\mathbb{Z}} a_0(m)\phi(p\cdot -m), \tag{21}$$

and define two sets of wavelets $\Psi=\{\psi_\ell\}_{\ell=1}^{1/b-1}, \widetilde{\Psi}=\{\widetilde{\psi}_\ell\}_{\ell=1}^{1/b-1}$ by

$$\psi_\ell(\cdot) = p\sum_{m\in\mathbb{Z}} a_\ell(m)\phi(p\cdot -m); \quad \widetilde{\psi}_\ell(\cdot) = p\sum_{m\in\mathbb{Z}} \widetilde{a}_\ell(m)\phi(p\cdot -m), \tag{22}$$

where the refinement and wavelet masks $\{a_\ell\}_{\ell=0}^{1/b-1}, \{\widetilde{a}_\ell\}_{\ell=0}^{1/b-1}$ are given by (16) and (17). By Theorem 1, two wavelet systems $X(\Psi), X(\widetilde{\Psi})$ defined by

$$X(\Psi) = \{p^{n/2}\psi_\ell(p^n\cdot -k)\}_{1\le\ell<1/b-1,n,k\in\mathbb{Z}}; \quad X(\widetilde{\Psi}) = \{p^{n/2}\widetilde{\psi}_\ell(p^n\cdot -k)\}_{1\le\ell<1/b-1,n,k\in\mathbb{Z}} \tag{23}$$

will form bi-frames for $L_2(\mathbb{R})$, if $\phi\in L_2(\mathbb{R})$ and two systems $X(\Psi)$ and $X(\widetilde{\Psi})$ are Bessel sequences.

COROLLARY 4. *Consider a finitely supported, real-valued, nonnegative window sequence $g\in\ell_2(\mathbb{Z})$ that satisfies (18). Then, the two wavelet systems $X(\Psi), X(\widetilde{\Psi})$ generated by (23) with the masks $\{a_\ell\}_{\ell=0}^{1/b-1}$ and $\{\widetilde{a}_\ell\}_{\ell=0}^{1/b-1}$ defined by (16) and (17) form bi-frames for $L_2(\mathbb{R})$.*

Proof. We first show that the refinable function ϕ with a refinement mask g satisfying (18) is in $L_2(\mathbb{R})$. The same conclusion for the case $p=2$ is proved in [5]. We start with showing that for any $\omega\in\mathbb{R}$,

$$\sum_{\mu=0}^{p-1} |\widehat{g}(\omega+\frac{2\pi\mu}{p})|^2 \le 1. \tag{24}$$

Note that

$$\sum_{\mu=0}^{p-1} |\widehat{g}(\omega+\frac{2\pi\mu}{p})|^2 = \sum_{\mu=0}^{p-1} |\sum_{m\in\mathbb{Z}} g(m)e^{-im(\omega+\frac{2\pi\mu}{p})}|^2 \le \sum_{\mu=0}^{p-1}\sum_{m\in\mathbb{Z}} |g(m)|^2 = \sum_{\mu=0}^{p-1}\sum_{j=0}^{p-1}\sum_{m\in\Omega_j} |g(m)|^2,$$

where $\Omega_j = (p\mathbb{Z}+j)\cap \mathrm{supp}(g)$. Since g is real-valued, nonnegative and satisfies (18), for any $0 \le j \le p-1$, we have

$$\sum_{n\in\Omega_j} |g(m)|^2 \le |\sum_{n\in\Omega_j} g(m)|^2 = \frac{1}{p^2}.$$

Therefore $\sum_{\mu=0}^{p-1} |\widehat{g}(\omega + \frac{2\pi\mu}{p})|^2 \le 1$.

Next, define

$$\widehat{f_n}(\xi) = \widehat{g}(p^{-1}\omega)\widehat{f_{n-1}}(p^{-1}\omega) = \prod_{j=1}^{n} \widehat{g}(p^{-j}\omega)\widehat{f}_0(p^{-n}\omega),$$

where $\widehat{f}_0 = \mathbb{1}_{[-\pi,\pi]}$. Recall that g is finitely supported and $\sum_{m\in\mathbb{Z}} g(m) = 1$. The pointwise limit $\widehat{\phi}$ of $\{\widehat{f_n}\}_n$ satisfies the refinement equation $\widehat{\phi}(p\omega) = \widehat{g}(\omega)\widehat{\phi}(\omega)$ with $\widehat{\phi}(0) = 1$, and ϕ is a compactly supported distribution. Furthermore,

$$\begin{aligned}
\|\widehat{f_n}\|^2 &= \int_{-\pi p^n}^{\pi p^n} |\prod_{j=1}^{n} \widehat{g}(p^{-j}\omega)|^2 d\omega \\
&= \int_{0}^{2\pi p^n} |\prod_{j=1}^{n} \widehat{g}(p^{-j}\omega)|^2 d\omega \\
&= \sum_{\mu=0}^{p-1} \int_{2\mu\pi p^{n-1}}^{2(\mu+1)\pi p^{n-1}} |\prod_{j=1}^{n} \widehat{g}(p^{-j}\omega)|^2 d\omega \\
&= \int_{0}^{2\pi p^{n-1}} |\prod_{j=1}^{n-1} \widehat{g}(p^{-j}\omega)|^2 \left(\sum_{\mu=0}^{p-1} |\widehat{g}(p^{-n}\omega + \frac{2\pi\mu}{p})|^2\right) d\omega.
\end{aligned}$$

Then by (24), we have

$$\|\widehat{f_n}\|^2 \le \int_{0}^{2\pi p^{n-1}} |\prod_{j=1}^{n-1} \widehat{g}(p^{-j}\omega)|^2 d\omega = \|\widehat{f_{n-1}}\|^2.$$

By induction,

$$\|\widehat{f_n}\|^2 \le \|\widehat{f}_0\|^2 = 2\pi,$$

for all $n \ge 0$. Since $\{\widehat{f_n}\}_n$ converges to $\widehat{\phi}$ pointwise, by Fatou's lemma,

$$\|\widehat{\phi}\|^2 \le \liminf_{n\to\infty} \|\widehat{f_n}\|^2 \le 2\pi,$$

and $\phi \in L_2(\mathbb{R})$.

Recall that all wavelet masks in $\Psi, \widetilde{\Psi}$ are finitely supported and have the first order vanishing moment, i.e., zero mean, as shown in [19], these two systems $X(\Psi), X(\widetilde{\Psi})$ are both Bessel sequences in $L_2(\mathbb{R})$. Consequently, by Theorem 1, the wavelet systems $X(\Psi)$ and $X(\widetilde{\Psi})$ form bi-frames for $L_2(\mathbb{R})$. □

In the next, we present several examples of window sequence g that satisfy the condition (18), which leads to MRA-based wavelet bi-frames for $L_2(\mathbb{R})$ generated by digital Gabor filters.

EXAMPLE 5 (refinement mask of linear B-spline). *Let g denote the refinement mask of linear B-spline function, i.e., $g = \frac{1}{4}[1,2,1]$. Then, define two sets of refinement and wavelet masks by (16) and(17)*

$$\begin{cases} a_0 = \frac{1}{4}[1,2,1], \\ a_1 = \frac{3}{16}[-1,2,-1] + i\frac{\sqrt{3}}{8}[1,0,-1], \\ a_2 = \frac{3}{16}[-1,2,-1] + i\frac{\sqrt{3}}{8}[-1,0,1]; \end{cases} \quad \text{and} \quad \begin{cases} \widetilde{a}_0 = \frac{1}{4}[1,2,1], \\ \widetilde{a}_1 = \frac{1}{6}[-1,2,-1] + i\frac{\sqrt{3}}{6}[1,0,-1], \\ \widetilde{a}_2 = \frac{1}{6}[-1,2,-1] + i\frac{\sqrt{3}}{6}[-1,0,1]. \end{cases}$$

Since g satisfies (18) with $p = 2$, The corresponding systems $X(\Psi)$ and $X(\widetilde{\Psi})$ form MRA-based dyadic wavelet bi-frames for $L_2(\mathbb{R})$.

EXAMPLE 6 (discretized general B-splines). *Let B_k^p denote the B-spline function of order k with the knots $\{0, p, \ldots, pk\}$. Then, it is known that the function B_k^p is a non-negative function with support $[0, pk]$ and satisfies*

$$\sum_{n\in\mathbb{Z}} B_k^p(\cdot - pn) = 1.$$

See [14] for more details. Thus, we have $\sum_{n\in\mathbb{Z}} \frac{1}{p} B_k^p(j - pn) = \frac{1}{p}$ for any integer j, which is equivalent to (18). Then, the two wavelet systems $X(\Psi), X(\widetilde{\Psi})$ generated by the two mask sets $\{a_\ell\}_{\ell=0}^{1/b-1}$ and $\{\widetilde{a}_\ell\}_{\ell=0}^{1/b-1}$ given by (16) and (17) form MRA-based p-dilation wavelet bi-frames for $L_2(\mathbb{R})$. For example, define a window sequence by sampling $\frac{1}{2}B_3^2$:

$$g = \frac{1}{96}[1, 8, 23, 32, 23, 8, 1].$$

By Theorem 3 and Corollary 4, the corresponding refinable function $\phi \in L_2(\mathbb{R})$, and the two wavelet systems $X(\Psi)$ and $X(\widetilde{\Psi})$ generated from g form dyadic wavelet bi-frames for $L_2(\mathbb{R})$. See Figure 1 for the graphs of two refinable functions and wavelets. Also, see Figure 2 for the illustration of 2D tensor product of refinement and wavelet masks, which show strong orientation selectivity.

EXAMPLE 7 (refinement masks of general B-splines). *A B-spline functions B_k^1 of order k with the knots $\{0, 1, ..., k\}$ is a refinable function with refinement mask*

$$g = \big[\frac{1}{2^{k+1}}\binom{k+1}{0}, \frac{1}{2^{k+1}}\binom{k+1}{1}, ..., \frac{1}{2^{k+1}}\binom{k+1}{k+1}\big].$$

It can be seen that the mask g defined above satisfies (18) with $p = 2$, i.e., $\sum_{n\in\Omega_j} g(n) = 1/2$, for all $j \in \mathbb{Z}/2\mathbb{Z}$, where $\Omega_j = (2\mathbb{Z} + j) \cap \mathrm{supp}(g)$. The corresponding refinable function $\phi = B_k^1 \in L_2(\mathbb{R})$ is a piecewise polynomial of degree $k-1$ in C^{k-2}, supported on $[0, k]$. By Theorem 3 and Corollary 4, the two wavelet systems $X(\Psi)$ and $X(\widetilde{\Psi})$ generated from g form dyadic wavelet bi-frames for $L_2(\mathbb{R})$. For example, consider the refinement mask

$$g = \frac{1}{8}[1, 3, 3, 1],$$

whose refinable function is the quadratic B-spline function, i.e. $\phi = B_2^1$.

Another example considers the refinement mask:

$$g = \frac{1}{16}[1, 4, 6, 4, 1],$$

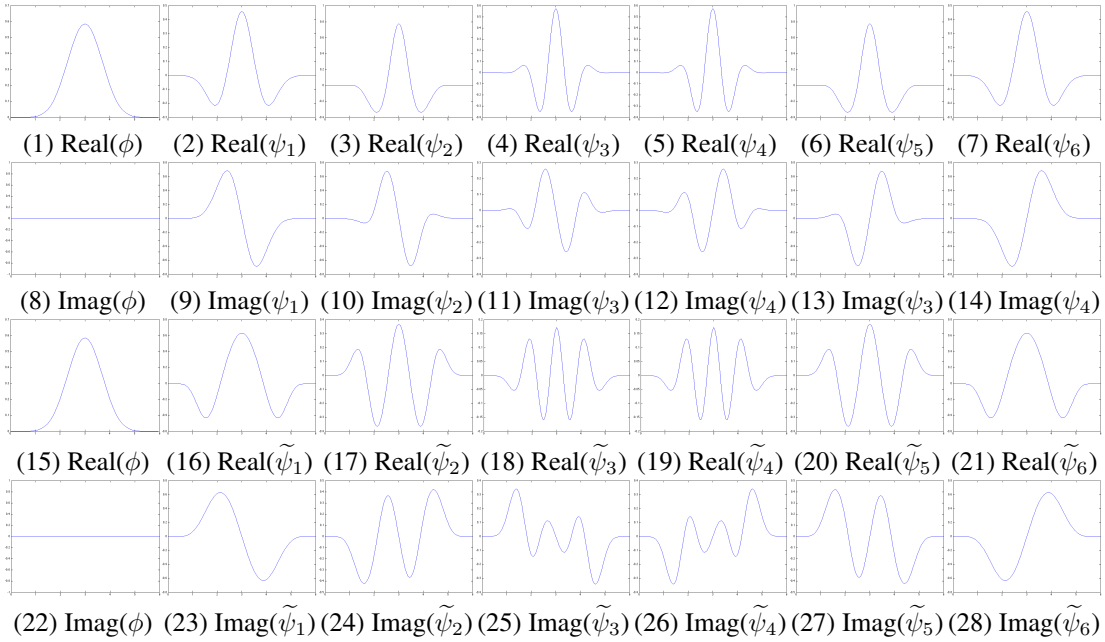

FIG. 1. *Real and imaginary parts of refinable and wavelet functions generated from discrete quadratic B-spline in Example 6.*

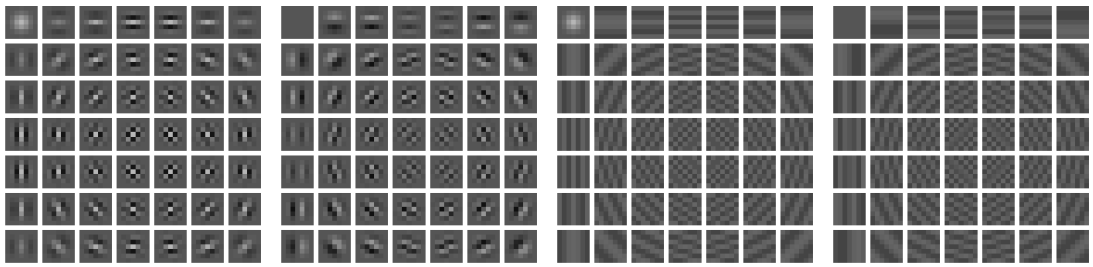

FIG. 2. *Real and imaginary parts of 2D tensor products of refinement and wavelet masks generated from discrete quadratic B-spline in Example 6.*

whose refinable function ϕ is the cubic B-spline function, i.e.

$$\phi = B_3^1 = \frac{x^3}{6}\chi_{[0,1)}(x) + \left(\frac{2}{3} - \frac{1}{2}x(x-2)^2\right)\chi_{[1,2)}(x) + \left(\frac{2}{3} - \frac{1}{2}(4-x)(x-2)^2\right)\chi_{[2,3)}(x) + \frac{(4-x)^3}{6}\chi_{[3,4)}(x), \tag{25}$$

where χ denotes the indicator function. In fact, the mask g can also be viewed as integer samples of $\frac{1}{2}B_2^2$. See Figure 3 for the graphs of two refinable functions and wavelets. Also, see Figure 4 for the illustration of 2D tensor product of refinement and wavelet masks, which show strong orientation selectivity.

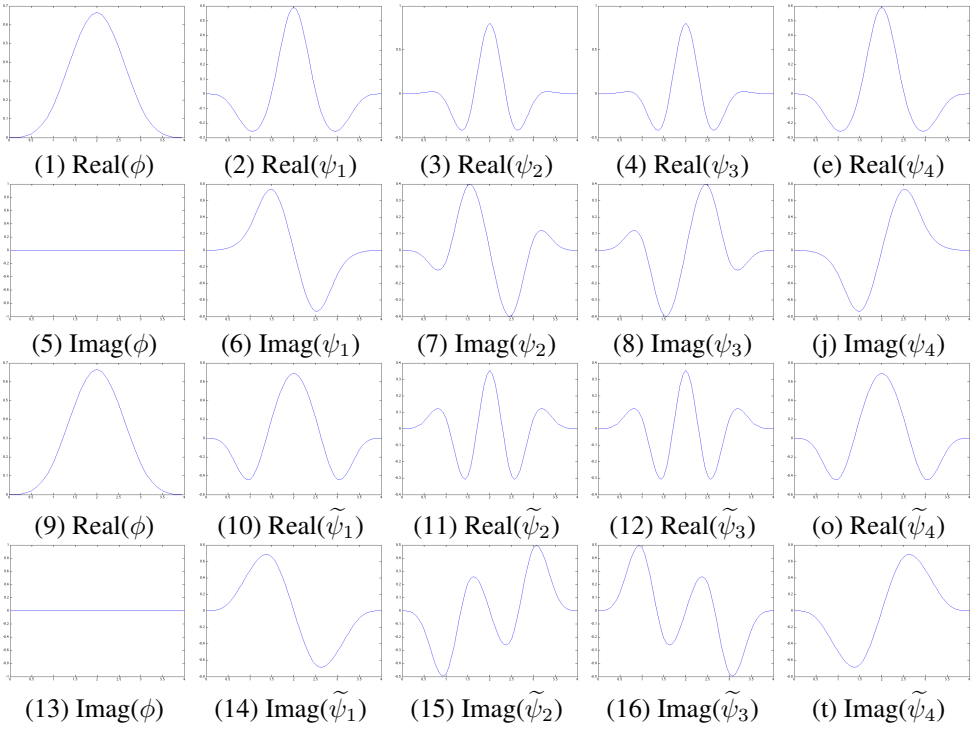

FIG. 3. *Real and imaginary parts of refinable and wavelet functions generated from cubic B-spline in Example 7.*

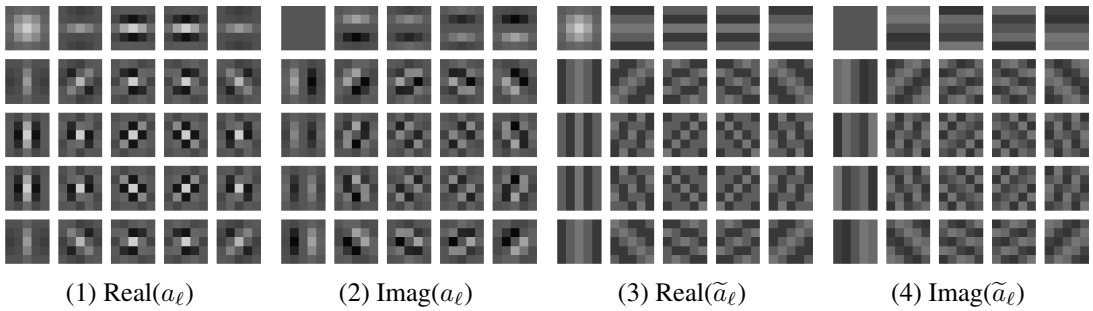

FIG. 4. *Real and imaginary parts of 2D tensor products of refinement and wavelet masks generated from cubic B-spline in Example 7.*

The construction scheme above can be extended to $L_2(\mathbb{R}^d)$ in a straightforward manner. Suppose that we can construct a finitely supported, nonnegative window sequence $g \in \ell_2(\mathbb{Z}^d)$ that satisfies

$$\sum_{\mathbf{m}\in\Omega_j} g(\mathbf{m}) = \frac{1}{p^d}. \tag{26}$$

for all $j \in \mathbb{Z}^d/p\mathbb{Z}^d$, where $\Omega_j = (p\mathbb{Z}^d + j) \cap \mathrm{supp}(g)$. Then, the masks $\{a_\ell\}$ and $\{\widetilde{a}_\ell\}$ defining (23) will satisfy (12) in high-dimensional setting, and the resulting two systems $X(\{a_\ell\}), X(\{\widetilde{a}_\ell\})$ form MRA-based p-dilation wavelet bi-frames for $L_2(\mathbb{R}^d)$.

EXAMPLE 8 (refinement mask of box spline). *Consider the box spline of three directions*

$$\{(1,0)^\top,(0,1)^\top,(1,1)^\top\},$$

whose refinement mask is

$$g=\frac{1}{8}\begin{pmatrix}0&1&1\\1&2&1\\1&1&0\end{pmatrix}. \tag{27}$$

It can be seen that such a window function g satisfies the condition (26) with $p=2$. The wavelet masks is then give by

$$a_1=\begin{pmatrix}0&\frac{3}{32}&-\frac{3}{32}-\frac{\sqrt{3}}{16}i\\-\frac{3}{32}+\frac{\sqrt{3}}{16}i&\frac{3}{16}&-\frac{3}{32}-\frac{\sqrt{3}}{16}i\\-\frac{3}{32}+\frac{\sqrt{3}}{16}i&\frac{3}{32}&0\end{pmatrix},\quad a_2=\begin{pmatrix}0&\frac{3}{32}&-\frac{3}{32}+\frac{\sqrt{3}}{16}i\\-\frac{3}{32}-\frac{\sqrt{3}}{16}i&\frac{3}{16}&-\frac{3}{32}+\frac{\sqrt{3}}{16}i\\-\frac{3}{32}-\frac{\sqrt{3}}{16}i&\frac{3}{32}&0\end{pmatrix},$$

$$a_3=\begin{pmatrix}0&-\frac{3}{32}+\frac{\sqrt{3}}{16}i&-\frac{3}{32}+\frac{\sqrt{3}}{16}i\\\frac{3}{32}&\frac{3}{16}&\frac{3}{32}\\-\frac{3}{32}-\frac{\sqrt{3}}{16}i&-\frac{3}{32}-\frac{\sqrt{3}}{16}i&0\end{pmatrix},\quad a_4=\begin{pmatrix}0&-\frac{3}{32}+\frac{\sqrt{3}}{16}i&\frac{3}{32}\\-\frac{3}{32}+\frac{\sqrt{3}}{16}i&\frac{3}{16}&-\frac{3}{32}-\frac{\sqrt{3}}{16}i\\\frac{3}{32}&-\frac{3}{32}-\frac{\sqrt{3}}{16}i&0\end{pmatrix},$$

$$a_5=\begin{pmatrix}0&\frac{3}{64}-\frac{\sqrt{3}}{16}i&\frac{3}{64}+\frac{\sqrt{3}}{16}i\\\frac{3}{64}+\frac{\sqrt{3}}{16}i&-\frac{9}{32}&\frac{3}{64}-\frac{\sqrt{3}}{16}i\\\frac{3}{64}-\frac{\sqrt{3}}{16}i&\frac{3}{64}+\frac{\sqrt{3}}{16}i&0\end{pmatrix},\quad a_6=\begin{pmatrix}0&-\frac{3}{32}-\frac{\sqrt{3}}{16}i&-\frac{3}{32}-\frac{\sqrt{3}}{16}i\\\frac{3}{32}&\frac{3}{16}&\frac{3}{32}\\-\frac{3}{32}+\frac{\sqrt{3}}{16}i&-\frac{3}{32}+\frac{\sqrt{3}}{16}i&0\end{pmatrix},$$

$$a_7=\begin{pmatrix}0&\frac{3}{64}+\frac{\sqrt{3}}{16}i&\frac{3}{64}-\frac{\sqrt{3}}{16}i\\\frac{3}{64}-\frac{\sqrt{3}}{16}i&-\frac{9}{32}&\frac{3}{64}+\frac{\sqrt{3}}{16}i\\\frac{3}{64}+\frac{\sqrt{3}}{16}i&\frac{3}{64}-\frac{\sqrt{3}}{16}i&0\end{pmatrix},\quad a_8=\begin{pmatrix}0&-\frac{3}{32}-\frac{\sqrt{3}}{16}i&\frac{3}{32}\\-\frac{3}{32}-\frac{\sqrt{3}}{16}i&\frac{3}{16}&-\frac{3}{32}+\frac{\sqrt{3}}{16}i\\\frac{3}{32}&-\frac{3}{32}+\frac{\sqrt{3}}{16}i&0\end{pmatrix},$$

and the dual wavelet masks is given by

$$\widetilde{a}_1=\begin{pmatrix}-\frac{1}{18}+\frac{\sqrt{3}}{18}i&\frac{1}{9}&-\frac{1}{18}-\frac{\sqrt{3}}{18}i\\-\frac{1}{18}+\frac{\sqrt{3}}{18}i&\frac{1}{9}&-\frac{1}{18}-\frac{\sqrt{3}}{18}i\\-\frac{1}{18}+\frac{\sqrt{3}}{18}i&\frac{1}{9}&-\frac{1}{18}-\frac{\sqrt{3}}{18}i\end{pmatrix},\quad \widetilde{a}_2=\begin{pmatrix}-\frac{1}{18}-\frac{\sqrt{3}}{18}i&\frac{1}{9}&-\frac{1}{18}+\frac{\sqrt{3}}{18}i\\-\frac{1}{18}-\frac{\sqrt{3}}{18}i&\frac{1}{9}&-\frac{1}{18}+\frac{\sqrt{3}}{18}i\\-\frac{1}{18}-\frac{\sqrt{3}}{18}i&\frac{1}{9}&-\frac{1}{18}+\frac{\sqrt{3}}{18}i\end{pmatrix},$$

$$\widetilde{a}_3=\begin{pmatrix}-\frac{1}{18}+\frac{\sqrt{3}}{18}i&-\frac{1}{18}+\frac{\sqrt{3}}{18}i&-\frac{1}{18}+\frac{\sqrt{3}}{18}i\\\frac{1}{9}&\frac{1}{9}&\frac{1}{9}\\-\frac{1}{18}-\frac{\sqrt{3}}{18}i&-\frac{1}{18}-\frac{\sqrt{3}}{18}i&-\frac{1}{18}-\frac{\sqrt{3}}{18}i\end{pmatrix},\quad \widetilde{a}_4=\begin{pmatrix}-\frac{1}{18}-\frac{\sqrt{3}}{18}i&-\frac{1}{18}+\frac{\sqrt{3}}{18}i&\frac{1}{9}\\-\frac{1}{18}+\frac{\sqrt{3}}{18}i&\frac{1}{9}&-\frac{1}{18}-\frac{\sqrt{3}}{18}i\\\frac{1}{9}&-\frac{1}{18}-\frac{\sqrt{3}}{18}i&-\frac{1}{18}+\frac{\sqrt{3}}{18}i\end{pmatrix},$$

$$\widetilde{a}_5=\begin{pmatrix}-\frac{1}{9}&\frac{1}{18}-\frac{\sqrt{3}}{18}i&\frac{1}{18}+\frac{\sqrt{3}}{18}i\\\frac{1}{18}+\frac{\sqrt{3}}{18}i&-\frac{1}{9}&\frac{1}{18}-\frac{\sqrt{3}}{18}i\\\frac{1}{18}-\frac{\sqrt{3}}{18}i&\frac{1}{18}+\frac{\sqrt{3}}{18}i&-\frac{1}{9}\end{pmatrix},\quad \widetilde{a}_6=\begin{pmatrix}-\frac{1}{18}-\frac{\sqrt{3}}{18}i&-\frac{1}{18}-\frac{\sqrt{3}}{18}i&-\frac{1}{18}-\frac{\sqrt{3}}{18}i\\\frac{1}{9}&\frac{1}{9}&\frac{1}{9}\\-\frac{1}{18}+\frac{\sqrt{3}}{18}i&-\frac{1}{18}+\frac{\sqrt{3}}{18}i&-\frac{1}{18}+\frac{\sqrt{3}}{18}i\end{pmatrix},$$

$$\widetilde{a}_7=\begin{pmatrix}-\frac{1}{9}&\frac{1}{18}+\frac{\sqrt{3}}{18}i&\frac{1}{18}-\frac{\sqrt{3}}{18}i\\\frac{1}{18}-\frac{\sqrt{3}}{18}i&-\frac{1}{9}&\frac{1}{18}+\frac{\sqrt{3}}{18}i\\\frac{1}{18}+\frac{\sqrt{3}}{18}i&\frac{1}{18}-\frac{\sqrt{3}}{18}i&-\frac{1}{9}\end{pmatrix},\quad \widetilde{a}_8=\begin{pmatrix}-\frac{1}{18}+\frac{\sqrt{3}}{18}i&-\frac{1}{18}-\frac{\sqrt{3}}{18}i&\frac{1}{9}\\-\frac{1}{18}-\frac{\sqrt{3}}{18}i&\frac{1}{9}&-\frac{1}{18}+\frac{\sqrt{3}}{18}i\\\frac{1}{9}&-\frac{1}{18}+\frac{\sqrt{3}}{18}i&-\frac{1}{18}-\frac{\sqrt{3}}{18}i\end{pmatrix}.$$

The resulting two wavelet systems $X(\Psi), X(\widetilde{\Psi})$ form dyadic non-separable bi-frames for $L_2(\mathbb{R}^2)$.

4. Multi-scale discrete wavelet bi-frames induced by Gabor filters and their frame properties. Once MRA-based wavelet bi-frames are constructed via the MEP, the K-level decomposition and reconstruction of discrete signals can be implemented by a filter bank based algorithm. The convolution of two sequences $f_1, f_2 \in \ell_2(\mathbb{Z})$, denoted by $f_1 \otimes f_2$, is defined pointwise by

$$(f_1 \otimes f_2)(m) = \sum_{n=-\infty}^{+\infty} f_1(n) f_2(m-n),\ m \in \mathbb{Z}.$$

Let $\downarrow_p$ denote the down-sampling operator defined by

$$(f\downarrow_p)(m) = f(pm),\ m \in \mathbb{Z},$$

and let $\uparrow_p$ denote the up-sampling operator defined by

$$(f \uparrow_p)(m) = f(m/p) \quad \text{if } m/p \in \mathbb{Z}, \text{ and } 0 \text{ otherwise.}$$

Then, for any signal $f \in \ell_2(\mathbb{Z})$, the K-level wavelet decomposition can be recursively computed as follows: $c_{0,0} = f$, and for $k = 1, \dots K$,

$$\begin{cases} c_{0,k} = \left(\sqrt{p} \cdot \overline{a_0(-\cdot)} \otimes c_{0,k-1}\right)\downarrow_p, \\ c_{\ell,k} = \left(\sqrt{p} \cdot \overline{a_\ell(-\cdot)} \otimes c_{0,k-1}\right)\downarrow_p, \quad \ell = 1, ..., 1/b-1. \end{cases} \tag{28}$$

The reconstruction of f from the coarsest-level low-pass coefficients $\{c_{0,K}\}$ and K-level high-pass wavelet coefficients $\{c_{\ell,k}\}_{1\le k\le K, 1\le \ell<1/b}$ is also done in the same recursive manner: for $k = K, K-1, ..., 1$,

$$c_{0,k-1} = \sqrt{p} \sum_{\ell=0}^{\frac{1}{b}-1} \widetilde{a}_\ell \otimes (c_{\ell,k} \uparrow_p), \tag{29}$$

and we have $f = c_{0,0}$.

From the cascade algorithm above, it can be seen that such a K-level wavelet decomposition expands the signal over a frame for $\ell_2(\mathbb{Z})$ defined by

$$\left\{\{\phi_K(\cdot - p^K j)\}_{j\in\mathbb{Z}}, \{\psi_{1,k}(\cdot - p^k j)\}_{1\le k\le K, j\in\mathbb{Z}}, \dots, \{\psi_{1/b-1,k}(\cdot - p^k j)\}_{1\le k\le K, j\in\mathbb{Z}}\right\}, \tag{30}$$

where $\phi_K, \psi_{\ell,k}$ are the sequences defined by

$$\widehat{\phi_K}(\omega) = \sqrt{p}\prod_{j=0}^{K-1} \widehat{a}_0(p^j\omega), \text{and} \quad \widehat{\psi_{\ell,k}} = \sqrt{p}\widehat{a}_\ell(p^{k-1}\omega)\prod_{j=0}^{k-1} \widehat{a}_0(p^j\omega),$$

for $\ell = 1, \dots, 1/b-1, k = 1, \dots, K$. The reconstruction is done over its dual frame defined by

$$\left\{\{\widetilde{\phi}_K(\cdot - p^K j)\}_{j\in\mathbb{Z}}, \{\widetilde{\psi}_{1,k}(\cdot - p^k j)\}_{1\le k\le K, j\in\mathbb{Z}}, \dots, \{\widetilde{\psi}_{1/b-1,k}(\cdot - p^k j)\}_{1\le k\le K, j\in\mathbb{Z}}\right\}, \tag{31}$$

where $\widetilde{\phi}_K, \widetilde{\psi}_{\ell,k}$ are the sequences defined by

$$\widehat{\widetilde{\phi}_K}(\omega) = \sqrt{p}\prod_{j=0}^{K-1} \widehat{\widetilde{a}}_0(p^j\omega), \text{and} \quad \widehat{\widetilde{\psi}_{\ell,k}} = \sqrt{p}\widehat{\widetilde{a}}_\ell(p^{k-1}\omega)\prod_{j=0}^{k-1} \widehat{\widetilde{a}}_0(p^j\omega),$$

for $\ell = 1, \ldots, 1/b - 1, k = 1, \ldots, K$.

From (28) and (29), the analysis operator $W : \ell_2(\mathbb{Z}) \to \ell_2(\mathbb{Z})$ of the discrete wavelet frame used in the K-level decomposition above can be written as a block matrix

$$W = \left(H_0^K, H_1 H_0^{K-1}, \ldots; H_{\frac{1}{b}-1} H_0^{K-1}, \ldots; H_1, \ldots, H_{\frac{1}{b}-1} \right)^\top,$$

and the synthesis operator $\widetilde{W}^* : \ell_2(\mathbb{Z}) \to \ell_2(\mathbb{Z})$ of its dual frame can also be written as a block matrix

$$\widetilde{W}^* = \left(\widetilde{H}_0^{*K}, \widetilde{H}_0^{*K-1} \widetilde{H}_1^*, \ldots, \widetilde{H}_0^{*K-1} \widetilde{H}_{\frac{1}{b}-1}^*, \ldots, \widetilde{H}_1^*, \ldots, \widetilde{H}_{\frac{1}{b}-1}^* \right).$$

Herein, H_ℓ and $\widetilde{H}_\ell^*$ $(0 \le \ell \le \frac{1}{b} - 1)$ are defined from the two sets of masks $\{a_\ell\}_{\ell=0}^{\frac{1}{b}-1}$ and $\{\widetilde{a}_\ell\}_{\ell=0}^{\frac{1}{b}-1}$ as follows,

$$H_\ell f = \left(\sqrt{p} \cdot \overline{a_\ell(-\cdot)} \otimes f \right) \downarrow_p, \quad \ell = 0, \ldots, b^{-1} - 1, \tag{32}$$

and

$$\widetilde{H}_\ell^* f = \sqrt{p}\, \widetilde{a}_\ell \otimes (f \uparrow_p), \quad \ell = 0, \ldots, b^{-1} - 1, \tag{33}$$

for any $f \in \ell_2(\mathbb{Z})$. When $K = 1$, the analysis operator and synthesis operator of the underlying dual frames have the following form:

$$W = \left(H_0, H_1, \ldots, H_{\frac{1}{b}-1} \right)^\top, \quad \text{and} \quad \widetilde{W}^* = \left(\widetilde{H}_0^*, \widetilde{H}_1^*, \ldots, \widetilde{H}_{\frac{1}{b}-1}^* \right). \tag{34}$$

The frame defined by (30) with the masks $\{a_\ell\}_{\ell=0}^{\frac{1}{b}-1}$ of the form (16) indeed can be viewed as a discrete Gabor induced frame for $\ell_2(\mathbb{Z})$ with K-level multi-scale structure. When $K = 1$, the frame defined by (30) is exactly a Gabor induced frames for $\ell_2(\mathbb{Z})$. Discrete wavelet bi-frames for $\mathbb{R}^N$ can be obtained via the same process where the convolution is done by periodic boundary extension.

MRA-based wavelet bi-frames for $\ell_2(\mathbb{Z})$ or $\mathbb{R}^N$ have the same efficient cascade algorithm for signal decomposition and signal reconstruction. One main difference between bi-frames and tight frame lies in the frame bound ratio, i.e., the ratio between upper frame bound and lower frame bound. As the upper and lower frame bounds are the supremum and infimum of the eigenvalues of the corresponding frame operator, the frame bound ratio can be viewed as the condition number of the frame operator, which measures the numerical stability when being used in applications. Tight frames have the lowest frame bound ratio 1. See Table 1 for the numerically computed frame bounds of sample wavelet frames and their dual frames in Example 5–7 for finite dimensional Euclidean space $\mathbb{R}^{1024}$. It can be seen that the frame bound ratios are all less than 2.5, and the frame bound ratios are nearly the same for multi-level frames and single-level wavelet frames with the same filter banks. Before ending the section, we give a theoretical estimation of frame bound ratios of single-level wavelet frames constructed in this paper for $\mathbb{C}^N$. For simplicity, the dilation factor p is assumed to be a factor of the dimensionality N.

For a matrix $Q \in \mathbb{C}^{M_1 \times N_1}$, let $\sigma(Q) = \sqrt{\lambda(Q^*Q)}$ denote the set of singular values of Q, where $\lambda(Q^*Q)$ denotes the set of eigenvalues of Q^*Q. Then $\|Q\|_2 = \sigma_{\max}(Q) = \sqrt{\lambda_{\max}(Q^*Q)}$ and $\|Q\|_2 \le \sqrt{\|Q\|_1 \|Q\|_\infty}$.

THEOREM 9 (frame bound ratio). *Consider single-level discrete wavelet frame X for $\mathbb{C}^N$ derived from the filter bank $\{a_\ell\}_{\ell=0}^{1/b-1}$ given by (16). Define $d_j = \frac{\left(\sum_{n \in \Omega_j} |\sqrt{p} g(n)|^2 \right)^{1/2}}{\sqrt{b}}$ for $j = 0, \ldots, p-1$, and define*

TABLE 1
frame bounds of sample discrete wavelet bi-frames constructed in Section 3 for $\mathbb{R}^{1024}$

lowpass		$[1,2,1]/4$	$[1,8,23,32,23,8,1]/96$	[1, 4, 6, 4, 1]/16	[1, 3, 3, 1]/8
original	level 1	1.1250/0.7500	1.6833/0.9919	1.3691/0.9453	1.3333/0.8000
	level 2	1.1250/0.7500	1.6871/0.9890	1.3697/0.9290	1.3659/0.7224
	level 3	1.1250/0.7500	1.6871/0.9881	1.3703/0.9234	1.3659/0.6981
dual	level 1	1.3333/0.8889	1.5067/0.8719	1.4604/0.7920	1.3333/0.8000
	level 2	1.3333/0.8889	1.6604/0.8707	1.5717/0.7903	1.4689/0.8048
	level 3	1.3333/0.8889	1.7099/0.8707	1.6194/0.7899	1.5172/0.8048

$\mu_\ell = \frac{|\sum_m g_\ell(m)|}{\sum_m g_0(m)}$ *if* $\sum_m g_\ell(m) \neq 0$*, and* 0 *otherwise, for* $\ell = 1, \ldots, 1/b-1$*. Then, the frame bound ratio of* X *is bounded above by*

$$(\frac{\max d_j}{\min d_j})^2 \left(\mu_{\text{sum}} + 1\right)^2 \left(\mu_{\max} + 1\right)^2,$$

where $\mu_{\max} = \max_{\ell \geq 1} |\mu_\ell|$, $\mu_{\text{sum}} = \sum_{\ell \geq 1} |\mu_\ell|$.

Proof. Let $G \in \mathbb{C}^{\frac{N}{pb} \times N}$ denote the analysis operator of the discrete single-level wavelet frame X derived from a Gabor filter bank $\{g_\ell\}_{\ell=1}^{\frac{1}{b}-1}$. By (34), the operator G is a block matrix

$$G = \left(H_0, H_1, \ldots, H_{\frac{1}{b}-1}\right)^\top,$$

where $H_\ell \in \mathbb{C}^{\frac{N}{p} \times N}$ denotes the matrix form of (32) with periodic boundary extension, for $0 \leq \ell \leq 1/b-1$.

For a Gabor filter bank whose window sequence g satisfying (18), we can split its corresponding analysis operator G into $G = \overline{G}D$, where $D \in \mathbb{C}^{N \times N}$ is a diagonal matrix with diagonal elements

$$(d_0, d_1, \cdots d_{p-1}, d_0, \cdots d_{p-1}, \cdots, d_0, \cdots d_{p-1}) \in \mathbb{C}^N,$$

with $d_j = \frac{\left(\sum_{n \in \Omega_j} |\sqrt{p} g(n)|^2\right)^{1/2}}{\sqrt{b}}$. Then, $\overline{G} \in \mathbb{C}^{\frac{N}{pb} \times N}$ is the analysis operator of the single-level wavelet frame defined from Gabor filter bank $\{\widetilde{g}_\ell(m) = \widetilde{g}(m) e^{-2\pi i \ell b m}, m = 0, \ldots, \frac{1}{b} - 1\}_{\ell=0}^{1/b-1}$ with window function $\widetilde{g} = (\frac{\sqrt{p} g(0)}{d_0}, \frac{\sqrt{p} g(1)}{d_1}, \cdots)$. It can be seen that $\widetilde{g}$ satisfies

$$\sum_{n \in \Omega_j} |\widetilde{g}(n)|^2 = b$$

for all $j \in \mathbb{Z}/p\mathbb{Z}$, where $\Omega_j = (p\mathbb{Z} + j) \cap \text{supp}(\widetilde{g})$. By Corollary 2 in [23], $\overline{G}$ is the analysis operator of a discrete Gabor tight frame, and thus $\overline{G}^* \overline{G} = I \in \mathbb{C}^{N \times N}$.

As shown in [23], the analysis operator W for the filter bank given by (16) can also be split into $W = CG$, where

$$C = \begin{pmatrix} I_{\frac{N}{p}} & & & \\ -\mu_1 I_{\frac{N}{p}} & e^{-i\theta_1} I_{\frac{N}{p}} & & \\ \cdots & & & \\ -\mu_{\frac{1}{b}-1} I_{\frac{N}{p}} & & & e^{-i\theta_{\frac{1}{b}-1}} I_{\frac{N}{p}} \end{pmatrix} \in \mathbb{C}^{\frac{N}{pb} \times \frac{N}{pb}},$$

and $I_{\frac{N}{p}}$ denotes the $\frac{N}{p} \times \frac{N}{p}$ identity matrix. Therefore, the analysis operator W can be written as

$$W = CG = C\overline{G}D.$$

Recall that the frame operator S is defined by $S = W^*W$. Then, the optimal frame bounds α, β are given by

$$\alpha = \|S^{-1}\|_2^{-1}, \quad \beta = \|S\|_2.$$

Therefore, we have the upper frame bound:

$$\|S\|_2 = \|W\|_2^2 \leq \|C\|_2^2 \|\overline{G}\|_2^2 \|D\|_2^2.$$

By the fact that $\overline{G}^*\overline{G} = I$,

$$\|S\|_2 \leq \|C\|_1 \|C\|_\infty \|D\|_2^2 = (\mu_{\text{sum}} + 1)\,(\mu_{\max} + 1)\, d_{\max}^2$$

where $\mu_{\max} = \max_{\ell \geq 1} |\mu_\ell|$, $\mu_{\text{sum}} = \sum_{\ell \geq 1} |\mu_\ell|$ and $d_{\max} = \max_{j=0,\ldots,p-1} d_j$.

For the lower frame bound, define the Hermitian matrices

$$Q = \overline{G}^* C^* C \overline{G}.$$

Then $S = W^*W = DQD$ and $S^{-1} = D^{-1}Q^{-1}D^{-1}$. Therefore,

$$\|S^{-1}\|_2 \leq \|D^{-1}\|_2^2 \|Q^{-1}\|_2 = \frac{1}{\lambda_{\min}(Q)} \|D^{-1}\|_2^2.$$

Note that $\overline{G}^*\overline{G} = I$. We may extend $\overline{G}$ to a unitary matrix $U = (\overline{G}, V)$ satisfying $U^*U = UU^* = I$. Then

$$U^*C^*CU = \begin{pmatrix} Q & \overline{G}^* C^* C V \\ V^* C^* C \overline{G} & V^* C^* C V \end{pmatrix}.$$

It can be observed that Q is a principal submatrix of U^*C^*CU. By the Cauchy interlace theorem of principal submatrices for hermitian matrices,

$$\lambda_{\min}(Q) \geq \lambda_{\min}(U^*C^*CU) = \lambda_{\min}(C^*C) = \frac{1}{\|(C^*C)^{-1}\|_2}.$$

The matrix C is a sparse matrix with a sparse inverse:

$$C^{-1} = \begin{pmatrix} I_{\frac{N}{p}} & \mathbf{0} & \cdots & \mathbf{0} \\ e^{i\theta_1}\mu_1 I_{\frac{N}{a}} & e^{i\theta_1} I_{\frac{N}{p}} & & \\ \vdots & & \ddots & \\ e^{i\theta_{\frac{1}{b}-1}}\mu_{\frac{1}{b}-1} I_{\frac{N}{p}} & & & e^{i\theta_{\frac{1}{b}-1}} I_{\frac{N}{p}} \end{pmatrix}.$$

Then

$$\frac{1}{\|S^{-1}\|_2} \geq \frac{\lambda_{\min}(Q)}{\|D^{-1}\|_2^2} \geq \frac{1}{\|D^{-1}\|_2^2 \|(C^*C)^{-1}\|_2} \geq \frac{1}{\|D^{-1}\|_2^2} \frac{1}{\|C^{-1}\|_1 \|C^{-1}\|_\infty} \geq \frac{d_{\min}^2}{(1+\mu_{\text{sum}})(1+\mu_{\max})},$$

where $d_{\min} = \min_{j=0,\ldots,p-1} d_j$. This gives the lower frame bound. Therefore, the frame bound ratio is bounded above by

$$\frac{d_{\max}^2}{d_{\min}^2} \left(\mu_{\text{sum}} + 1\right)^2 \left(\mu_{\max} + 1\right)^2. \qquad \square$$

It is noted that the upper bound of frame bound ratio given in Theorem 9 is independent of the dimension of the space. In particular, when the window sequence g is a constant sequence $\frac{1}{M}(1,...,1)$, all the high pass Gabor filters have zero DC offset. If p is a factor of M, then by Theorem 9, the frame bound ratio is 1. In other words, the corresponding wavelet bi-frames forms a tight frame for $L_2(\mathbb{R})$, as shown in [24].

5. Experiments on image deconvolution. In this section, the MRA-based wavelet bi-frames constructed in Section 3 are tested in sparsity-based regularization for one representative inverse problem, image deconvolution. The wavelet bi-frames used in the experiments are defined by considering the following window sequence:

$$g = \frac{1}{2^7}[1, 7, 21, 35, 35, 21, 7, 1],$$

which is the refinement mask of 6-th order B-spline function. Following the construction scheme stated in Theorem 3, we consider two-level dyadic discrete wavelet bi-frames with size $M = 8$. Then, the wavelet bi-frames for image space are generated by the tensor products of one dimensional discrete un-decimated wavelet bi-frames.

By concatenating the 2D image as a vector in $\mathbb{R}^N$, most image recovery problems are about solving a linear inverse problem:

$$f = Hu + n, \tag{35}$$

where f denotes available observation, u denotes true image, and n denotes noise. For image deconvolution, H is a circulant matrix generated from the blur kernel.

Let W and $\widetilde{W}$ denote the analysis operators for a pair of K-level discrete wavelet bi-frames, and let W^*, $\widetilde{W}^*$ denote the corresponding synthesis operators. In the experiments, the so-called balanced sparsity-based regularization ([37]) is used for image recovery, which estimates u by solving the following optimization problem:

$$\min_{\alpha} \frac{1}{2}\|HW^*\alpha - f\|_2^2 + \frac{\kappa}{2}\|(I - WW^*)\alpha\|_2^2 + \lambda\|\alpha\|_1, \tag{36}$$

where W denotes the analysis operator of a tight frame. For wavelet bi-frames with $\widetilde{W}^*W = I$, the optimization (36) is then reformulated as

$$\min_{\alpha} \frac{1}{2}\|H\widetilde{W}^*\alpha - f\|_2^2 + \frac{\kappa}{2}\|(I - W\widetilde{W}^*)\alpha\|_2^2 + \lambda\|\alpha\|_1.$$

The model can be effectively solved by the accelerated proximal gradient (APG) algorithm [37]. Denote $F_1(\alpha) = \frac{1}{2}\|H\widetilde{W}^*\alpha - f\|_2^2 + \frac{\kappa}{2}\|(I - W\widetilde{W}^*)\alpha\|_2^2$ and $F_2(\alpha) = \lambda\|\alpha\|_1$. In the APG algorithm, one needs to estimate the Lipschitz constant L of ∇F_1, which is not an trivial task in this case. Therefore, we consider to use the APG algorithm with a backtracking stepsize rule ([1]). Denote $Q_L(\alpha, x) = F_1(x) + \langle \alpha - x, \nabla F_1(x)\rangle + \frac{L}{2}\|\alpha - x\|_2^2 + F_2(\alpha)$. And define $p_L(x) = \mathcal{T}_{\lambda/L}(x - \frac{1}{L}\nabla F_1(x))$, where $\mathcal{T}_\delta(x) = [t_\delta(x_1), t_\delta(x_2), \ldots]^\top$ is the soft thresholding operator, with $t_\delta(x_i) = \frac{x_i}{|x_i|}\max\{0, |x_i| - \delta\}$. Then, the algorithm is explicitly stated as follows.

ALGORITHM 10. *Take $L_0 > 0$, some $\eta > 1$ and α_0. Set $x_1 = \alpha_0$, $t_1 = 1$. For $k = 1, 2, ...$, do the following iteration to generate α_k*

(1) Find the smallest nonnegative integer i_k such that with $\widetilde{L} = \eta^{i_k} L_{k-1}$

$$F_1(p_{\widetilde{L}}(x_k)) + F_2(p_{\widetilde{L}}(x_k)) \le Q_{\widetilde{L}}(p_{\widetilde{L}}(x_k), x_k).$$

(1) Barbara (2) Bowl (3) Cameraman (4) Lena

FIG. 5. *Four tested images*

(2) Set $L_k = \eta^{i_k} L_{k-1}$.
(3) Set $\alpha_k = p_{L_k}(x_k)$.
(4) Set $t_{k+1} = \frac{1+\sqrt{1+4t_k^2}}{2}$.
(5) Set $x_{k+1} = \alpha_k + \frac{t_k - 1}{t_{k+1}}(\alpha_k - \alpha_{k-1})$.

In the experiments, we always take $L_0 = 1$ and $\eta = 3/2$. Let $\widetilde{\alpha}$ be the output of the above iterations, we set $\widetilde{u} = \widetilde{W}^* \widetilde{\alpha}$ to be the solution to image deconvolution problem.

The experiments on image deconvolution are done as follows. The tested images are firstly convolved with a blur kernel and then added with Gaussian white noise. The standard deviation of noise is $\sigma = 3$ and four types of blur kernel are tested: (1) disk kernel of radius 3 pixels, (2) linear motion blur kernel of length 15 pixels and orientation 30°, (3) Gaussian kernel of size 15×15 pixels and standard derivation 2, and (4) averaging kernel of size 9×9 pixels. The parameters are uniformly set for all images: $\lambda = 0.14$ and $\kappa = 0.5$. The performance of image recovery is measured in terms of the PSNR value given by

$$\text{PSNR} = -20 \log_{10} \frac{\|u - \widetilde{u}\|}{255N},$$

where N denotes the total number of image pixels, u and $\widetilde{u}$ denote the true image and its estimation. The higher the PSNR value, the better the quality of the estimation.

In the first experiment, the results obtained using the wavelet bi-frames proposed in this paper are compared to that from several discrete systems widely used in image recovery. These systems include the system related to difference operators in the total variation (TV) regularization (see e.g. [39]), linear spline framelet [11], and dual-tree complex wavelet transform (DT-CWT) [35]. Both linear spline framelet and DC-CWT are tight frames. See Table 2 for the summary of the PSNR values of the results generated by different methods, and see Figure 6 for a visual illustration. It can be seen that in general, the bi-frames constructed in this paper outperformed the other systems by a noticeable margin. Such a performance gain is mostly from the strong orientation selectivity of Gabor filters and the multi-scale structures.

The second experiment is to compare the performance of three Gabor frames with multi-scale structures. In additional to the proposed bi-frames, one is the hybrid discrete Gabor frame proposed in [23], which gains multi-scale structures by considering the union of multiple discrete Gabor frames with varying window sizes. The other is the MRA-based wavelet tight frame generated from digital Gabor filters with constant window functions [24]. In the experiment, the hybrid discrete Gabor frame is generated from the cubic B-spline functions using $\{M = 7, a = 2, b = \frac{1}{7}\}$ and $\{M = 15, a = 4, b = \frac{1}{15}\}$, where M denotes window size. The MRA-based wavelet tight frame is generated by window sequence $\frac{1}{8}[1, 1, 1, 1, 1, 1, 1, 1]$ and $p = 2$. See Table 3 for the summary of the PSNR values of the results obtained from these three Gabor systems, and see Figure 6 for a visual illustration. It can be seen that the performance of the proposed bi-frames is

TABLE 2
PSNR values of deblurred results for blurred images with noise level $\sigma = 3$

image	kernel	TV	linear spline framelet [11]	DT-CWT [35]	proposed bi-frames
Barbara512	disk	24.77	25.17	25.15	25.50
	motion	24.64	24.97	25.00	25.46
	Gaussian	24.13	24.14	24.19	24.24
	average	23.99	24.03	24.07	24.21
Bowl256	disk	28.73	28.92	28.99	29.26
	motion	28.88	29.08	29.15	29.62
	Gaussian	27.96	27.82	28.32	28.36
	average	28.73	28.84	28.94	29.24
Cameraman256	disk	26.31	26.83	26.22	27.11
	motion	26.18	27.14	26.35	27.02
	Gaussian	24.96	24.84	24.73	25.07
	average	25.08	25.12	25.00	25.39
Lena512	disk	32.05	32.17	32.25	32.75
	motion	30.86	30.49	31.21	31.57
	Gaussian	31.34	31.26	31.59	31.88
	average	30.10	29.96	30.21	30.36

slightly better than that of the Gabor-induced tights frames [24], and is comparable to the hybrid discrete Gabor frames [23]. Such an observation is not surprising as these three systems are all Gabor systems with multi-scale structures. The tight frames proposed in [24] are generated by digital Gabor filters with constant windows functions. The non-smoothness of window function often leads to a small performance loss in image recovery. The hybrid discrete Gabor frames [24] are not MRA-based, and thus do not have fast cascade algorithm for signal decomposition and reconstruction as the proposed bi-frames do.

5.1. Conclusions. In this paper, we studied the problem of bi-frames that have both multi-scale structures and good joint time-frequency resolution. It is shown that there exist a class of digital Gabor filters with fast decay in frequency domain that can generate MRA-based wavelet bi-frames. Together with fast cascade implementation of decomposition/reconstruction, such MRA-based wavelet bi-frames generated by digital Gabor filters can see their potentials in many applications.

REFERENCES

[1] A. BECK AND M. TEBOULLE, *A fast iterative shrinkage-thresholding algorithm for linear inverse problems*, SIAM J. Imaging Sci., 2 (2009), pp. 183–202.
[2] B. BOASHASH, ed., *Time-Frequency Signal Analysis*, Weiley Halsted Press, 1992.
[3] J. CAI, R. CHAN, AND Z. SHEN, *A framelet-based image inpainting algorithm*, Appl. Comput. Harmon. Anal., 24 (2008), pp. 131–149.
[4] J. CAI, H. JI, C. LIU, AND Z. SHEN, *Framelet based blind image deblurring from a single image*, IEEE Trans. Image Process., 21 (2012), pp. 562–572.
[5] A. CHAI AND Z. SHEN, *Deconvolution: A wavelet frame approach*, Numerische Mathematik, 106 (2007), pp. 529 – 587.
[6] O. CHRISTENSEN, *Frames and bases: An introductory course*, Springer Science & Business Media, 2008.
[7] A. COHEN, I. DAUBECHIES, AND J.-C. FEAUVEAU, *Biorthogonal bases of compactly supported wavelets*, Comm. Pure Appl. Math., 45 (1992), pp. 485–560.
[8] I. DAUBECHIES, *Orthonormal bases of compactly supported wavelets*, Comm. Pure Appl. Math., 40 (1988), pp. 909–996.

TABLE 3
PSNR values of deblurred results for blurred images with noise level $\sigma = 3$

image	kernel	Gabor tight frame [24]	hybrid Gabor frame [23]	proposed Gabor bi-frames
Barbara512	disk	25.48	25.65	25.50
	motion	25.49	25.70	25.46
	Gaussian	24.18	24.21	24.24
	average	24.10	24.27	24.21
Bowl256	disk	29.13	29.35	29.26
	motion	29.36	29.67	29.62
	Gaussian	28.46	28.66	28.36
	average	29.21	29.25	29.24
Cameraman256	disk	26.73	27.01	27.11
	motion	26.72	26.93	27.02
	Gaussian	24.94	25.04	25.07
	average	25.30	25.55	25.39
Lena512	disk	32.06	32.53	32.75
	motion	30.45	31.43	31.57
	Gaussian	31.55	31.74	31.88
	average	30.06	30.36	30.36

[9] I. DAUBECHIES, *The wavelet transform, time-frequency localization and signal analysis*, IEEE Trans. Inform. Theory, 36 (1990), pp. 961–1005.

[10] I. DAUBECHIES, A. GROSSMAN, AND Y. MEYER, *Painless non-orthogonal expansions*, J. Math. Phys., 45 (1986), pp. 1271–1283.

[11] I. DAUBECHIES, B. HAN, A. RON, AND Z. SHEN, *Framelets: MRA-based constructions of wavelet frames*, Appl. Comput. Harmon. Anal., 14 (2003), pp. 1–46.

[12] I. DAUBECHIES, H. LANDAU, AND Z. LANDAU, *Gabor time-frequency lattices and the Wexler-Raz identity*, J. Fourier Anal. Appl., 4 (1994), pp. 437–478.

[13] J. DAUGMAN, *Complete discrete 2-D Gabor transforms nby neural network for iimage analysis and compression*, IEEE T. Acoust. Speech., (1988).

[14] C. DE BOOR, *B (asic)-spline basics*, Mathematics Research Center, University of Wisconsin-Madison, 1986.

[15] B. DONG, J. LI, AND Z. SHEN, *X-ray ct image reconstruction via wavelet frame based regularization and radon domain inpainting*, J. Sci. Comput., 54 (2013), pp. 333–349.

[16] B. DONG AND Z. SHEN, *Image restoration: a data-driven perspective*, in Proc. ICIAM, L. Guo and Z. Ma, eds., High Education Press, Beijing, 2015, pp. 65–108.

[17] Z. FAN, A. HEINECKE, AND Z. SHEN, *Duality for frames*, J. Fourier Anal. Appl., (2015).

[18] D. GABOR, *Theory of communication*, J. IEE, 93 (1946), pp. 429–457.

[19] B. HAN, *Compactly supported tight wavelet frames and orthonormal wavelets of exponential decay with a general dilation matrix*, J. Comput. Appl. Math., 155 (2003), pp. 43–67.

[20] A. K. JAIN AND F. FARSHID, *Unsupervised texture segmentation using gabor filters*, Pattern Recogn., 24 (1991), pp. 1167–1186.

[21] A. JANSSEN, *Duality and biorthogonality for Weyl-Heisenberg frames*, J. Fourier Anal. Appl., 1 (1994), pp. 403–436.

[22] A. JANSSEN, *From continuous to discrete Weyl-Heisenberg frames through sampling*, J. Fourier Anal. Appl., 3 (1997), pp. 583–596.

[23] H. JI, Z. SHEN, AND Y. ZHAO, *Directional frames for image recovery: multi-scale discrete Gabor frames*, J. Fourier Anal. Appl., (2016), pp. 1–29.

[24] H. JI, Z. SHEN, AND Y. ZHAO, *Digital Gabor filters do generate MRA-based wavelet tight frames*, Appl. Comput. Harmon. Anal., In Press (2017).

[25] T. S. LEE, *Image representation using 2D Gabor wavelets*, IEEE Trans. Pattern Anal., 18 (1996), pp. 959–971.

[26] M. LI, Z. FAN, H. JI, AND Z. SHEN, *Wavelet frame based algorithm for 3d reconstruction in electron microscopy*, SIAM J.

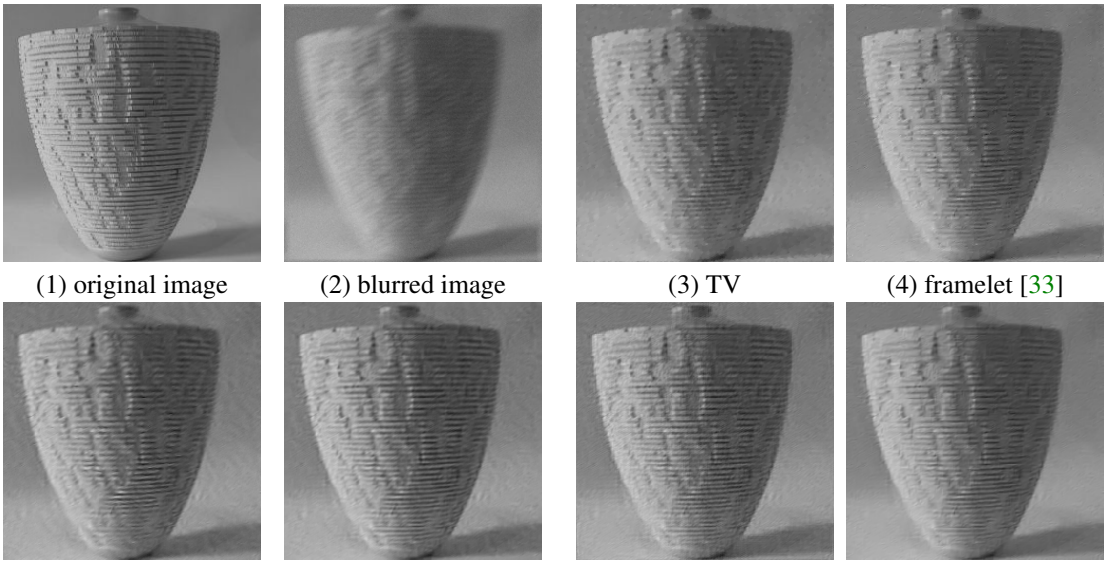

FIG. 6. *Visual illustration of image deconvolution. (a) true image; (b) image blurred by motion kernel and added by noise with noise level $\sigma = 3$; (c)-(h) deblurred results by different methods.*

Sci. Comput., 36 (2014), pp. B45–B69.
[27] S. LI, *On general frame decompositions*, Numer. Func. Anal. Opt., 16 (1995), pp. 1181–1191.
[28] S. MALLAT, *Multiresolution approximations and wavelet orthonormal bases of $L^2(R)$*, Trans. Amer. Math. Soc., 315 (1989), pp. 69–87.
[29] Y. MEYER, *Wavelets and operators*, vol. 1, Cambridge university press, 1995.
[30] A. RON AND Z. SHEN, *Frames and stable bases for subspaces of $L_2(\mathbb{R}^d)$: the duality principle of Weyl-Heisenberg sets*, in Proceedings of the Lanczos Centenary Conference, M. Chu, R. Plemmons, D. Browns, and D. Ellison, eds., Raleigh, NC, 1993, pp. 422–425.
[31] A. RON AND Z. SHEN, *Affine system in $L_2(R^d)$: the analysis of the analysis operator*, J. Funct. Anal., 148 (1997).
[32] A. RON AND Z. SHEN, *Affine systems in $L_2(\mathbb{R}^d)$ II: Dual systems*, J. Fourier Anal. Appl., 3 (1997), pp. 617–637.
[33] A. RON AND Z. SHEN, *Weyl-Heisenberg Frames and Riesz Bases in $L^2(R^d)$*, Duke Math. J., 89 (1997), pp. 237–282.
[34] A. RON AND S. Z., *Frames and stable bases for shift invariant subspaces of $l_2(r^d)$*, Canadian Journal of Mathematics, 47 (1995), pp. 1051 – 1094.
[35] I. W. SELESNICK, R. G. BARANIUK, AND N. C. KINGSBURY, *The dual-tree complex wavelet transform*, IEEE Signal Proc. Mag., 22 (2005), pp. 123–151.
[36] Z. SHEN, *Wavelet frames and image restorations*, in Proc. ICM, vol. 4, Hindustan Book Agency, India, 2010, pp. 2834–2863.
[37] Z. SHEN, K.-C. TOH, AND S. YUN, *An accelerated proximal gradient algorithm for frame-based image restoration via the balanced approach*, SIAM J. Imaging Sci., 4 (2011), pp. 573–596.
[38] P. L. SØNDERGAARD, *Gabor frames by sampling and periodization*, Adv. Comput. Math., 27 (2007), pp. 355–373.
[39] Y. WANG, J. YANG, W. YIN, AND Y. ZHANG, *A new alternating minimization algorithm for total variation image reconstruction*, SIAM J. Imaging Sci., 1 (2008), pp. 248–272.
[40] J. WEXLER AND S. RAZ, *Discrete gabor expansions*, Signal Process., 21 (1990), pp. 207–220.